GEOPHYSICS, VOL. 82, NO. 4 (JULY-AUGUST 2017); P. D199–D209, 13 FIGS., 2 TABLES.
10.1190/GEO2016-0203.1

Electrical properties and its correlation to the petrology of the Upper Yangtze organic shales

Lanfang He[1], Ling Chen[2], Xuben Wang[3], Zhengjiang Wang[4], Bing Zhang[3], Ligui Xu[5], Xuejun Liu[5], Weili Li[5], and Rujun Chen[6]

ABSTRACT

Shale gas is a particularly important research target on Chinese energy resources, especially in the Upper Yangtze region. Complex topography and geologic conditions challenge seismic exploration of shale gas in this area, and ground-based electromagnetic (EM) methods are used to aid recognition of the best reservoirs. However, the electrical properties of organic shale (EPOS) and its correlation to shale-gas petrology remain poorly understood. We studied EPOS and their correlation to shale petrology by measuring and analyzing the petrochemical features and complex impedance of rock samples from the Silurian Longmaxi and Cambrian Niutitang Formations in the Upper Yangtze, southwest China. Our study indicates that the organic shale in the Upper Yangtze features low resistivity and high polarizability in terms of a high negative phase, but no obvious low resistivity is observed among shaly sandstone and shales with lower and higher total organic carbon. Pyrite and quartz contents in the organic shale dominantly contribute to the EPOS with different mechanisms. Our result indicates that the EPOS bear relations to the petrology parameters of organic shale, which is essential for shale-gas evaluation and exploration. The correlation between EPOS and the shale-gas petrology promoted a new way for shale-gas exploration with complex geology, topography, and surface conditions in China, especially in the Upper Yangtze region, by using the ground-based EM method to evaluate the parameters of shale gas and to aid to delimit the productive reservoirs (“sweet spots”).

INTRODUCTION

Shale-gas resources continue to be a growing part of total gas production in the world (Miller and Shanley, 2010). Companies globally are aggressively pursuing these resources, hoping to find an opportunity like the Barnett Shale, a classic shale-gas system in the Fort Worth Basin, Texas (Loucks and Ruppel, 2007; Alexander et al., 2011). Outside of the United States, China has a huge potential wealth of shale-gas resources, including the world’s largest technically recoverable reserves, estimated at approximately 1115 Tcf (U.S. Energy Information Administration, 2013; Li et al., 2016). Research into shale gas, as well as an associated research and development upsurge, has been sparked by progress in the exploration, petrology, and geochemistry of these reserves in recent years (Zhang et al., 2007; Wang et al., 2012, 2016b; Ji et al., 2015; Zou et al., 2015; Gai et al., 2016; Li et al., 2016; Pan et al., 2016; Tang et al., 2016; Yan et al., 2016). Although shale gas has been reported from Paleozoic (Cambrian) through to Triassic rocks in China (Zou et al., 2015), more than half of all recoverable reserves are located on the Upper Yangtze Platform in southwest China; the shale-reserve opportunities here are attractive for research and investment across China and the Western world (U.S. Energy Information Administration, 2013; Pan et al., 2016).

Manuscript received by the Editor 18 April 2016; revised manuscript received 5 January 2017; published online 26 May 2017.
[1]Formerly BGP, China National Petroleum Corporation, Zhuozhou, China; presently State Key Laboratory of Lithospheric Evolution, Institute of Geology and Geophysics, Chinese Academy of Sciences, Beijing, China. E-mail: mofoo@263.net.
[2]State Key Laboratory of Lithospheric Evolution, Institute of Geology and Geophysics, Chinese Academy of Sciences, Beijing, China and CAS Center for Excellence in Tibetan Plateau Earth Sciences, Beijing, China. E-mail: lchen@mail.iggcas.ac.cn.
[3]State Key Laboratory of Oil and Gas Reservoir Geology and Exploitation, Chengdu University of Technology, Chengdu, China. E-mail: wxb@cdut.edu.cn; 575890321@qq.com.
[4]Chengdu Institute of Geology and Mineral Resources, CGS, Chengdu, China. E-mail: wzjcf825@163.com.
[5]BGP, China National Petroleum Corporation, Zhuozhou, China. E-mail: xuligui@bgp.com.cn; liuxuejun@cnpc.com.cn; liweili@cnpc.com.cn.
[6]Central South University, School of Geosciences and Info-Physics, Changsha, China. E-mail: chrujun@csu.edu.cn.

However, the complex geology, topography, and surface conditions of this region continue to hinder exploration, in particular seismic prospecting, of shale gas in the Upper Yangtze. Geoelectromagnetic methods, including magnetotellurics and time-frequency electromagnetics, are often used for shale-gas prospecting (Zhang et al., 2013; Min et al., 2014; Zhou et al., 2015). Electrical properties of the organic shale, the foundation of electromagnetic (EM) methods for shale exploration, play an important role for shale-gas reservoir assessment.

Geoelectromagnetic methods dominated oil and gas prospecting before the maturation of seismic-reflection approaches (Rust, 1940; Pirson, 1971; Zonge, 1972; Nekut and Spies, 1989; He et al., 2010; Zhdanov, 2010), and they remain one of the primary means of oil and gas exploration, in addition to logging (Meju, 2002; He et al., 2010; Zhdanov, 2010). Correlation between electrical properties and petrology has been researched for more than 100 years, and are widely accepted as tools for understanding and interpreting geoelectromagnetic data (Fox, 1830; Parkhomenko, 1967; Latovikova, 1983; Passey et al., 1990; Ulrich and Slater, 2004; Slater et al., 2005; Karato and Wang, 2013). However, electrical properties have not been widely used to evaluate the organic shale until recently. The electrical properties and its mechanism of the organic shale are also incompletely understood (Passey et al., 2010; Hart et al., 2011; Zhu et al., 2011; Yan et al., 2014). Organic shale is a type of black shale with a total organic carbon (TOC) greater than 2% (Yu et al., 2014, 2016; Liu et al., 2015; Zhou et al., 2015). In one study, Passey et al. (2010) discuss organic-shale resistivity and differences in interpretation, including how fluid saturation, clay, and pyrite contents might play roles to decrease the resistivity response if their volumes are sufficient. Resistivity R of organic shale increases with TOC following a $\Delta \times \lg R$ to TOC relationship, a deviation from conventional reservoir models that has been corroborated by other results (Kumar and Hoversten, 2012; Polish Geological Institute, 2012; Adao et al., 2015). Several case studies have shown that organic-rich shales with high polarizability and low resistivity are characteristic of the Upper Yangtze Platform, and laboratory sample complex resistivity measurements and compositional analysis demonstrate that pyrite plays an important role in decreasing resistivity in these sediments (Zhang et al., 2013; Li et al., 2014; Min et al., 2014; Xiang et al., 2014; Yan et al., 2014; Liu et al., 2015; Yu et al., 2015, 2016; Zhou et al., 2015). Nevertheless, there is still much work to be done to formulate and refine a model to properly interpret correlation between resistivity and the petrology of shale.

In this paper, we study the electrical properties and their correlation to the petrology and geochemistry of organic-shale samples (OSH) from the Silurian Longmaxi and Cambrian Niutitang Formations in the Upper Yangtze Platform, southwest China. We introduce the geologic setting and describe sample preparations. We then discuss methods for complex impedance measurement, whole rock and clay mineral analysis, and TOC measurement. The results of complex resistivity, phase and their correlation to TOC, Py, clay and brittle mineral content, especially the quartz content are showed and discussed.

GEOLOGIC SETTING AND SAMPLING

All of our samples were taken from the marine shales of the Longmaxi and Niutitang Formation on the Upper Yangtze Platform, southwest China. The Yangtze Platform is a major geologic unit in China that extends from west to east of southern China, from Yunnan to Jiangsu province (Figure 1). Sedimentary rocks are well-developed on this platform. These rocks are mainly composed with carbonates and cherts with great thicknesses, and they are widely exposed and stable in the Yangtze Platform (Yang et al., 2003). The western portion of the Yangtze Platform is called the Upper Yangtze, and it contains the Sichuan Basin and the surrounding area. The Sichuan Basin is a large basin in China and it is famous by its natural gas production (Pan et al., 2015). Marine organic-rich shales were widely developed in China during the Sinian period, but apart from Sichuan Basin, most of these marine shales have undertaken strong deformation during uplift (Pan et al., 2015; Yan et al., 2016). Consequently, a series of horst and graben basins were formed by tectonic activities, with the latter creating favorable settings for hydrocarbon enrichment. By the beginning of the Early Cambrian, the Yangtze area was a continental sea, and a large segment of the Yangtze block was covered with carbonate platforms that were subsequently drowned by a deep, muddy shelf system as a result of the global "Niutitang event" transgression (Li et al., 2015; Yan et al., 2016). Water depth in this sea gradually increased eastward, and sediments deposited to form the Niutitang Formation are dominated by the associations of dark shales, siliceous rocks, and shales interbedded with siltstones because of oxygen-poor deep waters (Yan et al., 2016). We sampled the Niutitang shale from the Cen'gong block, located to the southwest of Tongren city, in the northeast of Guizhou province (site 2 in Figure 1). The Niutitang shale developed stably, has a thickness that varies from 50 to 70 m across the study area, and is mainly composed of gray-to-black and siliceous shales with high TOC contents ranging from 1.6 wt%

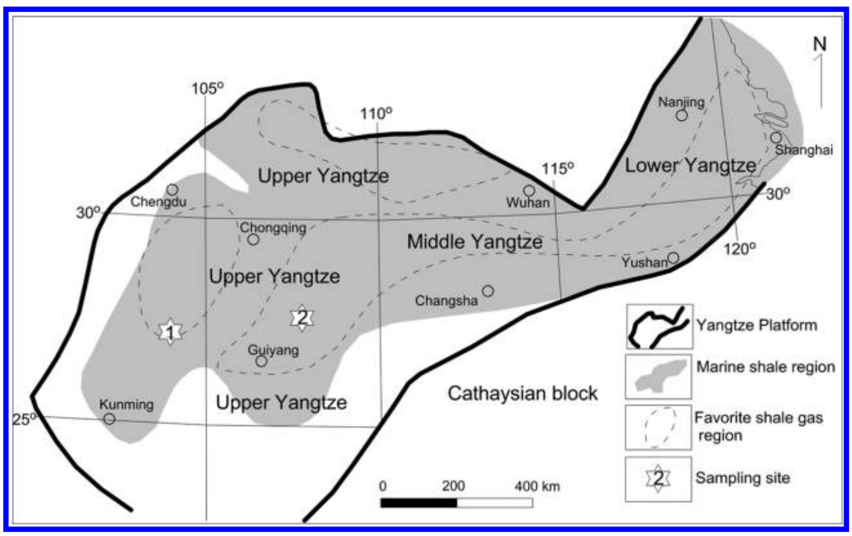

Figure 1. Regional geologic setting of the study area. South China consists of the Yangtze Platform and the Cathaysian block. Marine shales are widely developed on the Yangtze Platform and are important for gas exploration. We sampled the Longmaxi shale along the southern margin of the Sichuan Basin (site 1), to the northeast of Kunming, and the Niutitang shale from the Cen'gong block (site 2) to the northeast of Guiyang.

to 9.6 wt% and with R_o (thermal maturity) greater than 2.2% (Wang et al., 2016a).

In the Early Silurian, the Upper Yangtze region was located in the center of three major paleohighs that allowed for the deposition of deep-water calcareous shales in the southern Sichuan region, and deep-water siliceous shales in the eastern-northern Sichuan regions (Zou et al., 2015). The Longmaxi marine shale, a complex of organic-rich black shales, developed as a result of this partially closed marine-basinal environment (Pan et al., 2015). The Lower Silurian Longmaxi Formation is a black shale containing graptolites distributed across the upper-middle Yangtze area; it has a cumulative thickness between 50 and 600 m, TOC values from 1.0% to 7.3% (average of 2.1%), and R_o between 2.81% and 3.11% (average of 2.95%) (Zhang et al., 2007; Wang et al., 2012). We sampled the Longmaxi shale in the southern margin of the Sichuan Basin (site 1 in Figure 1), to the south of Yibin and the north of Zhaotong city, adjacent to Sichuan and Yunan provinces.

All of the samples in this stage are collected from the outcrops. We sampled more than 60 limestone, sandstone, mudstone, basalt, and shale samples in total; the static electrical properties of all samples are listed by Zhang et al. (2013). We measured the mineralogical contents and TOC for 25 of them, and 15 of them have measurement results for mineralogical contents, TOC, and impedance (complex resistivity and phase), but 1 of them has uncertain data and needs to be confirmed in future testing; 14 of them are discussed in this paper. We prepared shale and sand samples by cutting them into regular cubes with a length between 4 and 15 cm, a width between 2 and 10 cm, and a height between 2 and 6 cm, depending on the nature of cores. The remainder of the sample after cutting was divided into several portions for thin sectioning, TOC and R_o testing, and scanning electron microscopy. To preserve the natural contents of each rock samples, they were directly measured. No other processing, such as extraction of fluids from fissures and pores (Adao et al., 2015) or soaking, was done before the complex resistivity measurements.

DATA AND METHODS

Electrical property measurements

Complex resistivity measurements were taken on the prepared samples under room temperatures and pressures. Results are presented in terms of magnitude (resistivity) and phase or real and imaginary components of the impedance (Slater et al., 2005). All of the measurements were made using a four-pole electrode configuration, comprising two current electrodes and two potential electrodes (He et al., 2012; Adao et al., 2015). Two polymethyl methacrylate boxes, filled with copper sulfate mixed with wet flour dough, were used as the nonpolarizing electrode pair (Figure 2); the current electrodes were made of copperplate, the potential electrodes we used are the Ag-AgCl reference sensor pair. All complex resistivity measurements were carried out using a Solartron-1260A impedance/gain-phase analyzer (see AMETEK Inc. [2015] for detailed information on the precision and resolution of this analyzer) across a frequency range of 0.005−1000 Hz. The relative error of resistivity ranges from 1.40% to 3.97%, with an average mean of 2.68% between two measurements based on the result of one sample, and the relative error in phase ranges from 1.40% to 4.80% averages at 2.78%. To evaluate the difference between the four-pole electrode and the pole-pole configurations, we measured two samples using both configurations. Figure 3 shows the comparison result of four-pole and pole-pole configurations. Figure 3a shows the comparison of the modulus of Z ($|Z|$) in terms of the magnitude of the real and imaginary components of the impedance, their phase comparison is graphed in Figure 3b. The comparison result of sample 01 shows little difference between measured data from the two configurations. The relative error of $|Z|$ ranges from 0.29% to 0.69% with an average mean of 0.54%, and the relative error in phase ranges from 0.005% to 4.41% averages at 0.87%. Sample 02 has a greater average relative error of 5.59% and 4.95%. The reason is that sample 01 was measured 3 h later after it was set on the configuration, whereas sample 02 was measured shortly after it was set. The measurement system was not in a stable situation.

Whole rock and clay-mineral analysis

Whole rock and clay-mineral analysis are geochemical ways for determining the major and clay elements of the sedimentary rocks (Jackson et al., 1987). Classical whole rock and clay-mineral analysis methods include Fourier transform infrared spectroscopy and X-ray diffraction (XRD) analyses (Jackson et al., 1987). XRD is a kind of techniques that could be used for identifying rock and clay mineral by measuring and calculating the lattice parameters (d) of a specific mineral. The content of the identified mineral could be calculated by the intensity of the diffraction peaks. Figure 4 shows the XRD result of a sample for rock-mineral analysis, and the mineral contents of this sample based on the result of XRD are as follows: quartz ($d = 4.26$ and 3.34) 59.9%, plagioclase ($d = 3.20$) 8.3%, pyrite ($d = 2.71$) 7.1%, dolomite ($d = 2.89$) 1.8%, and total clay-mineral content 22.9%. The whole rock and clay-mineral compositions were measured with an XRD using a D/MAX 2500PC (Rigaku). Clay minerals with a diameter less than 2 μ were first separated using a centrifuge, and then relative quantitative and qualitative analysis were conducted under natural state conditions, at 550°C for 2 h. Samples were then saturated with ethylene glycol

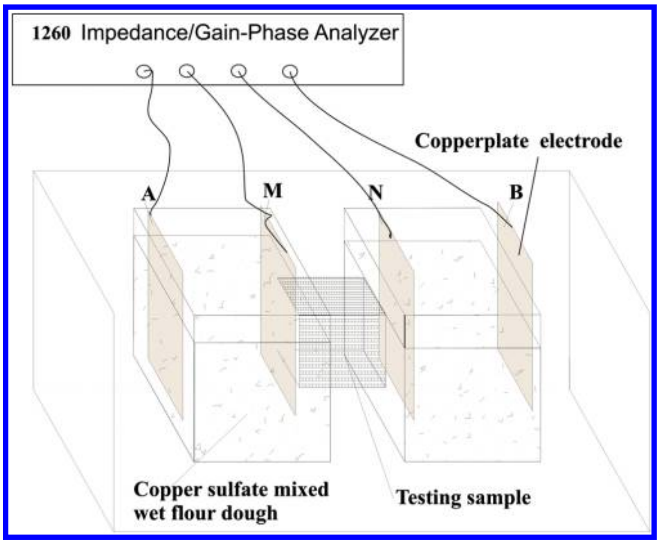

Figure 2. The map shows the laboratory system for complex impedance measurements, including the Solartron-1260A impedance/gain-phase analyzer that was used for impedance spectroscopy. This measurement system comprises a four-pole electrode configuration and was used across a frequency range of 0.005–1000 Hz, apart from two samples for configuration testing (0.005–10,000 Hz), as shown in Figure 3.

and retested at 60°C for 7 h. The operating voltage was 40 kV with a current of 100 mA, whereas the sweep speed was 6°/min for whole rock analysis and 4°/min for clay-mineral analysis.

TOC measurements

The TOC was measured using a CS230 carbon/sulfur determinator (LECO Corporation, 2008). The sample powder was soaked in dilute hydrochloric acid to dissolve inorganic carbon before measurement. The TOC was obtained by heating rocks in a high-frequency induction furnace and combusting organic matter to carbon dioxide. The liberated carbon dioxide was then measured using infrared spectroscopy, converted to TOC, and recorded as a mass weight percent of rock (McCarthy et al., 2011). For all measurements, the temperature was 23°C and humidity was 60%.

RESULTS AND DISCUSSION

We measured 14 samples in total, including 10 shale samples, 2 sandstone samples, 1 pyrite sample, and 1 coal sample. Eight OSH with TOC in the range 1.94%–7.41% are used to study organic-shale electrical properties and their correlation to its petrology. Two shaly sandstone samples (SST) and two black shale samples (BSH) with TOC lower than 1.0% are used as references for the OSH. The measurement results of mineralogical contents, TOC, resistivity, and phase variation for each sample are listed in Table 1. The samples have total brittle mineralogical content (TBC) ranges from 53.6% to 76.6%, which includes quartz (Qz), potash feldspar (Pf), plagioclase (Pl), calcite (Ca), and dolomite (Do). The total clay mineralogical content (TCC) ranges from 20.5% to 40.9%, and the TOC runs from 0.11% to 7.41%. The resistivity of the 12 samples features from 10 to 1000 Ωm. The phase (minus degree) ranges from –0.05° to −4.33°. The resistivity and phase values in Table 1 are the measured complex resistivity and phase result at frequency 0.01 Hz. One pyrite and one coal sample are measured to analyze the relationship between complex impedance results and TOC or Py. Understanding the correlation between the electrical properties of organic shale (EPOS) and the petrology of the organic shale is a key to interpret the EM data in shale-gas exploration. Factors such as water, clay, and pyrite in the shale are usually considered to be the main controls on the resistivity of shale-gas reservoirs, although in some cases, the rock may be much more electrically conductive

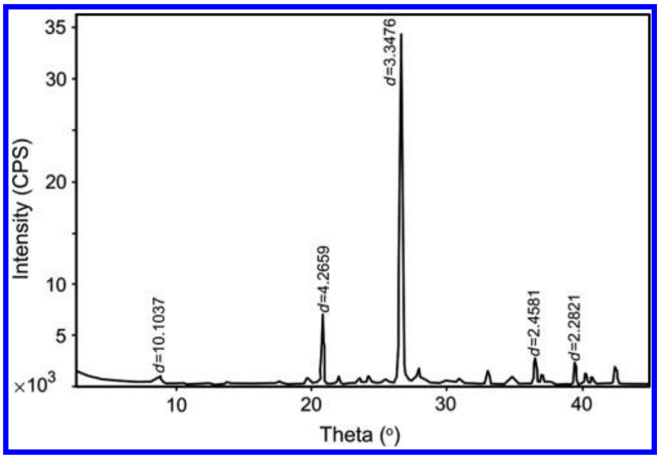

Figure 4. The XRD result of sample Q19 shows as an example for the whole rock-mineral analysis. Here, d means the lattice parameters of a specific mineral, which can be used to identify the mineral and can be determined using techniques such as XRD. The mineral contents of this sample are quartz ($d = 4.26$ and 3.34) 59.9%, plagioclase ($d = 3.20$) 8.3%, pyrite ($d = 2.71$) 7.1%, dolomite ($d = 2.89$) 1.8%, and total clay-mineral content 22.9%.

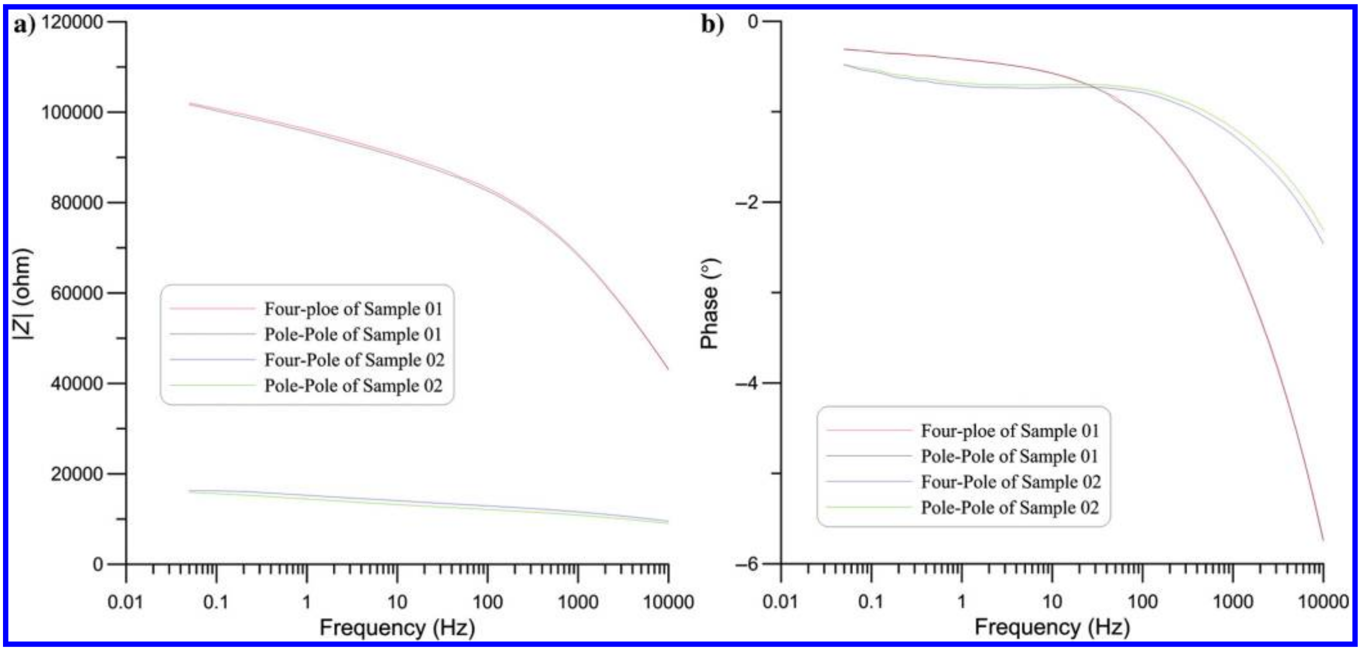

Figure 3. Comparison of the complex impedance measurement result using the four-pole and pole-pole configuration of two different samples (01 and 02). The four-pole configuration uses two current electrodes (A and B in Figure 2), and the other two are measurement electrodes (M and N in Figure 2). In the pole-pole configuration, A and B are used for current and measurement electrodes, respectively. (a) The comparison of the modulus of Z ($|Z|$) in terms of the magnitude of the real and imaginary components of the impedance. Their phase comparison is graphed in (b).

due to the presence of other mineral phases, such as graphite (Passey et al., 2010). In this section, we discuss the correlation of the components and EPOS of the Longmaxi and Niutitang Formations, which feature as low-resistivity and high-polarization anomalies, in the Upper Yangtze.

Electrical properties measurement results

Figure 5 shows the complex resistivity of the 12 (8 OSH, 2 SST, and 2 BSH) samples in the frequency range of 1000–0.005 Hz. The complex resistivity of the samples increases 1.2%–14% as the frequency decreases from 1000 to 0.005 Hz in the log-log scale. The resistivity of different dry samples ranges from 10 to 3000 Ωm. In general, organic shale has lower resistivity when compared with surrounding limestones and sandstones (Passey et al., 2010; Phillips, 2010; Zhang et al., 2013; Min et al., 2014; Yan et al., 2014; Adao et al., 2015). However, there are no obvious differences among the resistivity values of the OSH, the SST, and the BSH, for they are all fine-sediment rock containing clay, fine sandstone, and even organic matter. It is difficult to distinguish organic-shale formations from other permeable rock types, including sandstones, by their resistivity features, especially when they are fluid saturated.

Figure 6 shows the impedance phases of the 12 samples in the same frequency range. The phase value (minus degree) among the different samples ranges from 0.06° to 5.10° and from 1000 to 0.005 Hz. The result shows different behaviors among SST (Figure 6a), BSH (Figure 6b), and OSH (Figure 6c and 6d). From high (1000 Hz) to low frequency (0.005 Hz), the phases of SST gradually reduce from greater than 3.0° to less than 0.1°, the phases of BST gradually decrease from greater than 1.5° to less than 0.2° (in a frequency range from 1000 to 0.1 Hz), and slowly increase to 0.25° in the frequency range of 0.1–0.005 Hz. The phases of the first four OSH samples (Figure 6c, group 01) increase from approximately 0.1° to 1.5°–5.1° across the whole frequency range, 1000–0.005 Hz. In contrast, the phases of the other four OSH samples (Figure 6c, group 02) gradually decrease from greater than 0.7°–2.5° to less than 0.1°–1° in the frequency range 1000–1 Hz (one of them decrease at some 30 Hz), then gradually increase to 0.5°–1.7° and from 1 to 0.005 Hz.

Correlation between TOC and EPOS

In conventional reservoirs, the resistivity of a rock is directly related to electrically conductive components. Water is the primary

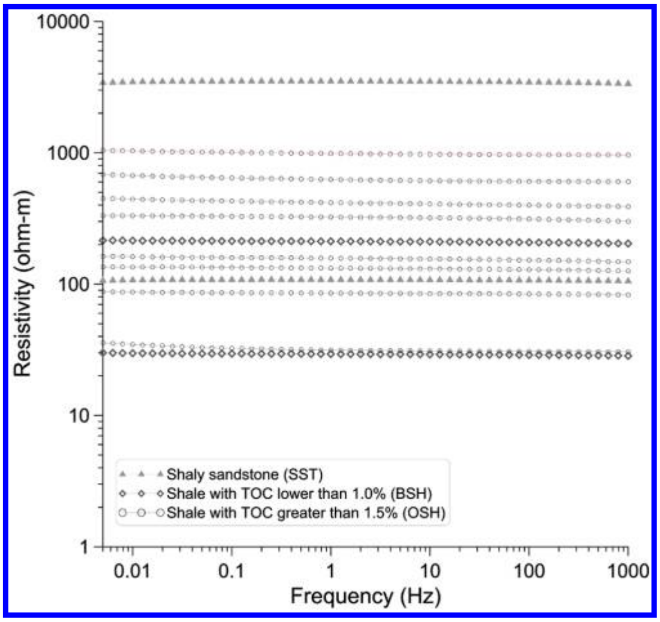

Figure 5. Complex resistivity of the 12 (eight OSH, two SST, and two BSH) samples in the frequency range of 1000–0.005 Hz. The resistivity value of the samples increases very slowly (1.2%–14%) as the frequency decreases from 1000 to 0.005 Hz.

Table 1. Measurement results of mineralogical contents, TOC, resistivity, and phase variation for each sample.[7]

Sample	Qz (wt%)	Pf (wt%)	Pl (wt%)	Ca (wt%)	Do (wt%)	Py (wt%)	He (wt%)	Gy (wt%)	TCC (wt%)	TBC (wt%)	TOC (%)	Lg (Res) (Ωm)	Phase (°)
SST01	18.6	10.9	26.7	0	0	—	14.8	—	29	56.2	0.11	2.03	−0.13
SST02	30.3	4.6	9.1	16.4	3.7	1	—	—	34.9	64.1	0.3	3.54	−0.05
BSH01	12.8	2.4	0	37.6	17.8	—	—	—	29.4	70.6	0.98	2.33	−0.14
BSH02	24.5	5.4	4.3	19.4	0	—	—	0.5	45.9	53.6	0.24	1.46	−0.26
OSH01	51.9	3.2	0	0	0	—	—	—	44.9	55.1	3.58	2.13	−0.44
OHS02	52.9	3.9	0	0	2.1	—	—	—	41.1	58.9	3.8	2.52	−0.58
OSH03	51.8	3.2	0	0	0	—	—	—	45	55	3.85	1.94	− 0.3
OSH04	36.7	0.6	3.2	26.3	9.8	2.9	—	—	20.5	76.6	4.33	2.21	−0.69
OSH05	61.2	1.3	7.9	0	0	7.2	—	—	22.4	70.4	4.7	2.65	− 1.5
OSH06	64.4	1.2	7.3	0	0	5.5	—	—	21.6	72.9	5.44	1.22	−1.36
OSH07	64.5	0	5.7	0	0	5.4	—	—	24.4	70.2	5.5	1.25	−2.21
OSH08	59.9	0	8.3	0	1.8	7.1	—	—	22.9	70	7.41	1.54	−4.33

[7]OSH, organic shale samples; SST, shaly sandstone samples; BSH, black shale samples with TOC lower than 1.0%; Qz, quartz; Pf, potash feldspar; Pl, plagioclase; Ca, calcite; Do, dolomite; Py, pyrite; He, hematite; Gy, gypsum; TCC, total clay-mineralogical content; TBC, total brittle-mineralogical content; TOC, total organic carbon; lg(Res), log 10 (resistivity). The resistivity and phase value in the table are the measured complex resistivity and phase result at the frequency of 0.01 Hz.

conductor of electricity in a rock, but nonconductive hydrocarbon fluids (i.e., oil or gas) always result in high resistivity as they displace water (Passey et al., 1990, 2010). In addition, the $\Delta \times \log R$-TOC model, which is proposed by Passey et al. (1990), indicates that the resistivity in log scale of a formation increases with increasing TOC. In shale-gas areas, the revised $\Delta \times \log R$ to the TOC model also indicates that resistivity increases with increasing TOC (Passey et al., 2010; Kumar and Hoversten, 2012). Adao et al. (2015) measure samples from the Haddessen well in Germany, and show a clear correlation that the electrical resistivity increases with increasing TOC. However, in the Upper Yangtze, several studies show that high-TOC shale samples from the Longmaxi and Niutitang Formations are characterized by low resistivity, as well as high polarization anomalies (Xiang et al., 2014; Li et al., 2015; Yu et al., 2016). Only a few studies consider the Longmaxi shale to have high resistivity (Wu et al., 2011).

Figure 7a shows the crossplot results of TOC and shale-sample resistivity; it shows that the resistivity generally decreases with the increasing of TOC because most samples with TOC greater than 5 wt% had resistivity lower than 100 Ωm. Resistivity log data (Figure 7b) from a shale-gas well also indicated that the resistivity of shale of the Longmaxi and Niutitang group decreases with increasing TOC. Based on the result shown in Figure 7, there is no obvious linear correlation between TOC and the resistivity in common logarithm scale. Figure 8 shows the correlation between TOC and the phase of the shale samples of Longmaxi and Niutitang group. The result shows a linear correlation between the phase and the TOC. The phase increases with the TOC increases. Shale sample with a TOC greater than 5% has a phase greater than 1.2°, those with a TOC less than 2% has a phase lower than 0.5°. We construct a simple model to formula the relation of TOC (Y) and the phase (X, in terms of minus degree) as

$$Y = X * \sin(70) + 3.4. \quad (1)$$

Comparison of the linear fit and measured result is posted in Figure 8; the standard fitting deviation of TOC is 1.22 wt%.

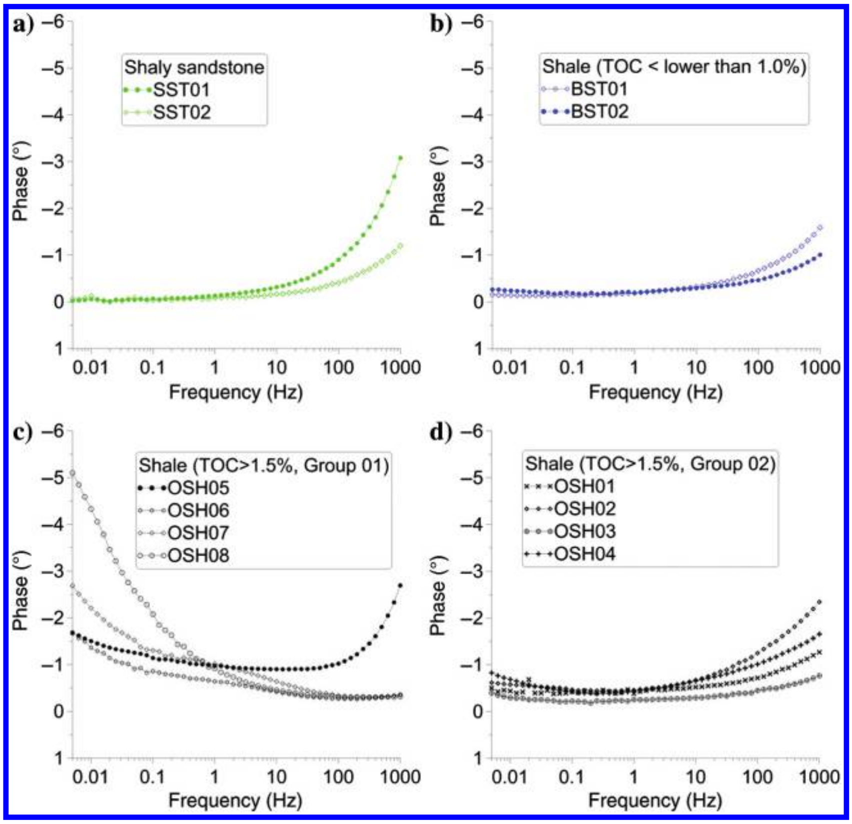

Figure 6. Impedance phases of the 12 (OSH01-08, SST01-02, and BSH01-02) samples in the frequency range of 1000–0.005 Hz. The phase means the phase shift between the real and imaginary components of the impedance. The phase value among the different samples ranges from 0.06° to 5.10°and from 1000 to 0.005 Hz. (a-d) Different phase variations with the frequency of SST, BSH, and OSH (two groups). In the frequency range from 1 to 0.05 Hz, the phase of OSH is greater than that of SST and BSH. (c and d) The different phase behaviors among eight OSH samples.

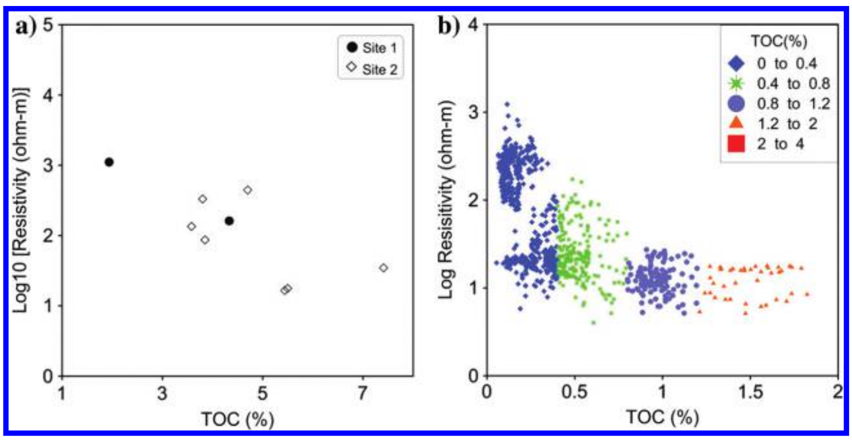

Figure 7. Correlation between the TOC and resistivity of the (a) samples and (b) the log data indicates a trend of that resistivity decrease with increasing TOC. The resistivities of the samples are the measured result at the frequency of 0.01 Hz.

Correlation between the pyrite content and EPOS

Pyrite plays a significant role in shale resistivity because it is characterized by very low resistivity and high polarizability, and it is commonly present in organic-rich intervals of shale formations due to the reducing conditions that enhance organic-matter preservation (Passey et al., 2010; Yu et al., 2014; Xiang et al., 2016). In many cases, pyrite contained in organic-rich intervals is used to interpret the low resistivity and high polarizability of the marine shale (Luo and Zhang, 1987; Xiang et al., 2014; Yan et al., 2014; Yu et al., 2014; Liu et al., 2015). Six of 13 samples contain pyrite greater than the limit of detection (LOD), and the correlation of the pyrite and the resistivity and phase is shown in Figure 9. This shows that the pyrite weight content has a negative relation to the resistivity and a positive relation to the phase of the samples apart from one discordant result. This sample (OSH05 as marked in the ellipse) has a lower TOC (4.7%) than the other one (TOC 7.41%), which has similar pyrite content; we do not know the reason that why it is discordant at this stage.

Figure 10 shows a comprehensive result on the relations among the TOC, pyrite, and phase variation with the frequency. Results of a pyrite-enriched sample without TOC, and a coal sample with 21% TOC contains pyrite lower than LOD are plotted in the same figure for reference to illustrate the effects of pyrite and TOC. As the figure shows, the pyrite-enriched sample is dominant with a value of greater than 3° at frequency ranges from 0.005 to 1 Hz, and it has a phase as high as 8.5°. The phase of the pyrite increases with the decreasing frequency. Two OHS samples follow the behavior of the pyrite-enriched sample. The other OHS samples have a phase of 0.5°–1.5° in the frequency range from 1 to 0.005 Hz. The phase of the coal sample is dominant for higher frequencies 1000–10 Hz, and it decreases with decreasing frequency. The OSHs feature lower phases than the coal sample at frequency ranges greater than 1 Hz and feature lower phases than the pyrite sample at frequency ranges lower than 100. The phase of the OSH increases with the decreasing frequency range lower than 1 Hz, and it has a clearer positive correlation to TOC than to pyrite content.

Correlation between the brittle and clay-mineral contents and EPOS

The brittle and clay-mineral contents are the key parameters to evaluate the gas shale, they control gas enrichment by means of controlling the porosity and microstructure and production due to their behaviors in the hydrofracturing (Bowker, 2007; Hill et al., 2007; Nie et al., 2009). As a result, the correlation between the brittle and clay-mineral contents and EPOS plays an important role in the evaluation of the gas shale using the EM methods. The relation of the resistivity against weight percent for brittle and clay-mineral contents of eight OSH samples is plotted in Figure 11. These results show that there is no clear relationship between resistivity and total brittle (Figure 11a) and clay (Figure 11b) mineral content. Regarding the relation between resistivity and quartz contents (Figure 11c), there has a trend that the resistivity decreases with the increasing quartz contents. Figure 11d shows a trend that the phase of the OSH increases with the increasing quartz content.

Quartz, as well as TOC, is a resistant mineral and leads to high resistivity in shale. It is difficult to understand the resistivity deceasing with increasing TOC and quartz content directly based on the mineral resistivity of organic matter and quartz in organic shale. Clay and quartz contents are important in controlling the porosity of the rock (Kuila et al., 2014). Jin et al. (2016) observed that the quartz content is positively correlated to porosity. Our results indicate that the quartz content is negatively correlated with clay content in the organic shales of the Longmaxi and Niutitang Formations in the Upper Yangtze (Figure 12). Result of different samples from the Chengdu University of Technology shows that the porosity, which is in terms of pore volume (cm^3/g), bears a negative correlation to the clay content of OSH in the Upper Yangtze as shown in Figure 13. The pore volume was measured by the nitrogen-adsorption method (Seaton and Walton, 1989). This indicates that the quartz content underlies the positive correlation to porosity of organic shale, and it strongly suggests that the quartz content increasing might lead to lower shale resistivity by affecting the porosity. Decreasing resistivity with increasing TOC is the result of increasing pyrite content and porosity, which is due to the quartz increasing, not organic material, in the Upper Yangtze. Although the physical and chemical mechanisms that generate the low-frequency phases of clays are still debated (Okay et al., 2014), there is strong

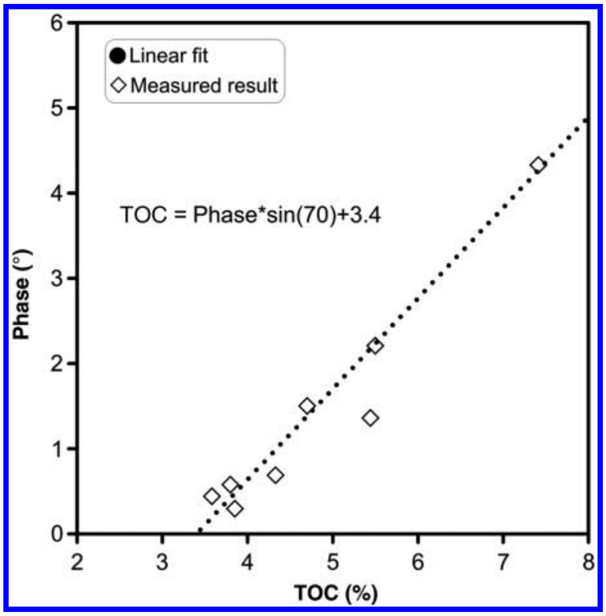

Figure 8. Correlation between TOC and the phase of the shale samples of Longmaxi and Niutitang group. The result indicates a linear correlation under the formula shown in the figure; the calculated results are shown as the black dot, and the standard fitting deviation of TOC between the calculated and the measured results is 1.22 wt%. The phase values are the measured result at the frequency of 0.01 Hz.

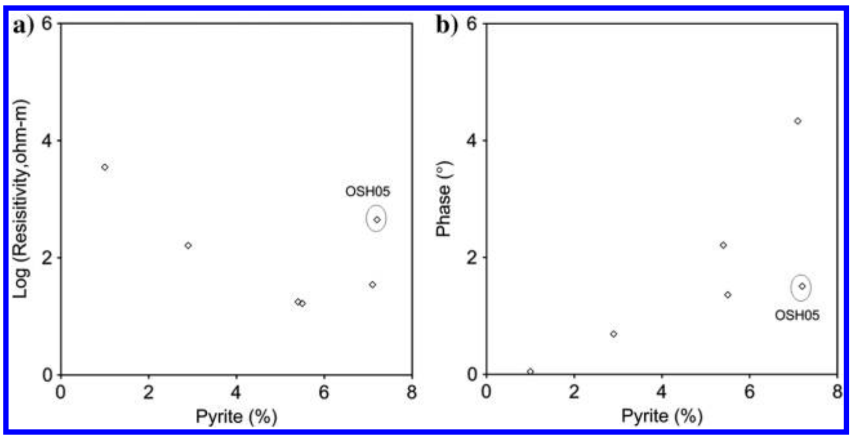

Figure 9. Correlation of the (a) pyrite and the resistivity and (b) phase shows a negative relation to the resistivity and a positive relation to the phase of the samples apart from one discord sample (OSH05). The resistivity and phase values are the measured result at the frequency of 0.01 Hz.

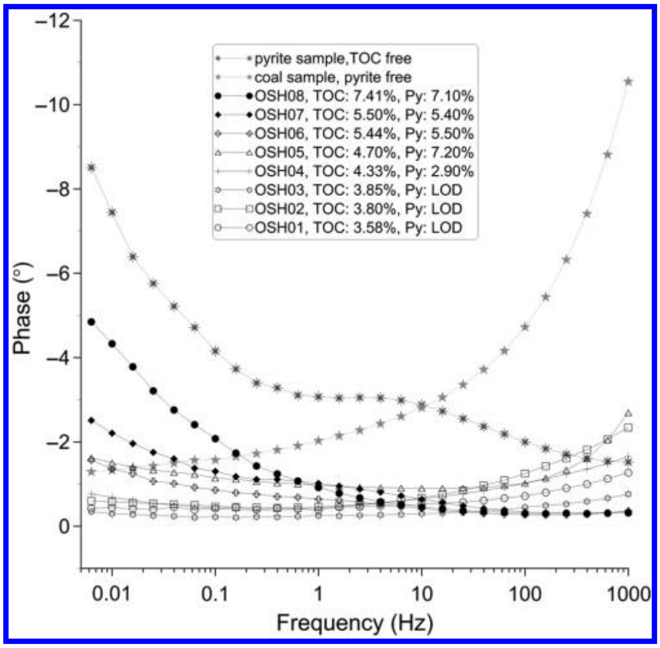

Figure 10. Crossplot of the comprehensive result on the relations among the TOC, pyrite, and phase variation with the frequency. Pyrite-enriched sample without TOC, and a coal sample with 21% TOC, are plotted as a reference to illustrate the effects of pyrite and TOC. The phase behavior of eight OSH, pyrite, and coal is shown in terms of their variation with frequency. LOD means lower than the limit of detection.

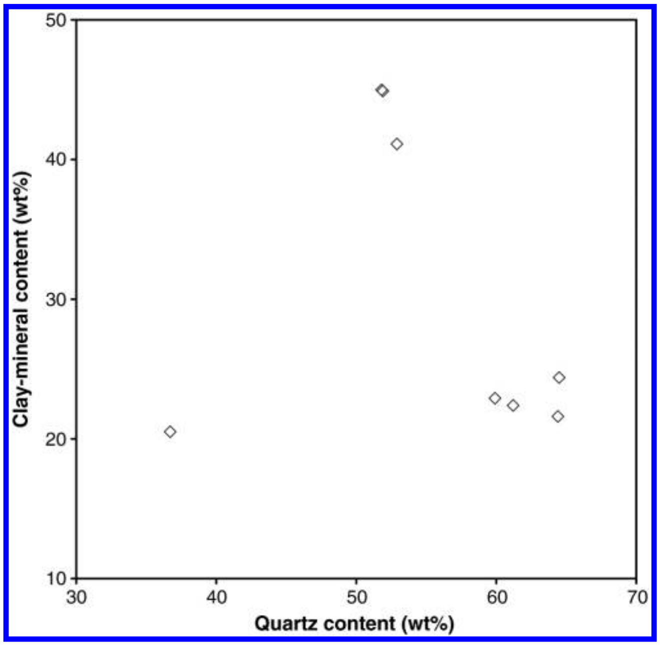

Figure 12. Correlation between the quartz content and the clay content in the OSH samples of the Longmaxi and Niutitang Formations in the Upper Yangtze.

Figure 11. Relation of the resistivity and phase against weight percent for brittle and clay mineral contents of eight OSH samples. (a and b) The relation between the resistivity and total brittle and clay-mineral content. (c) The relation between the resistivity and quartz contents and (d) relation between the phase and the quartz contents of the OSH. The resistivity and phase values are the measured result at the frequency of 0.01 Hz.

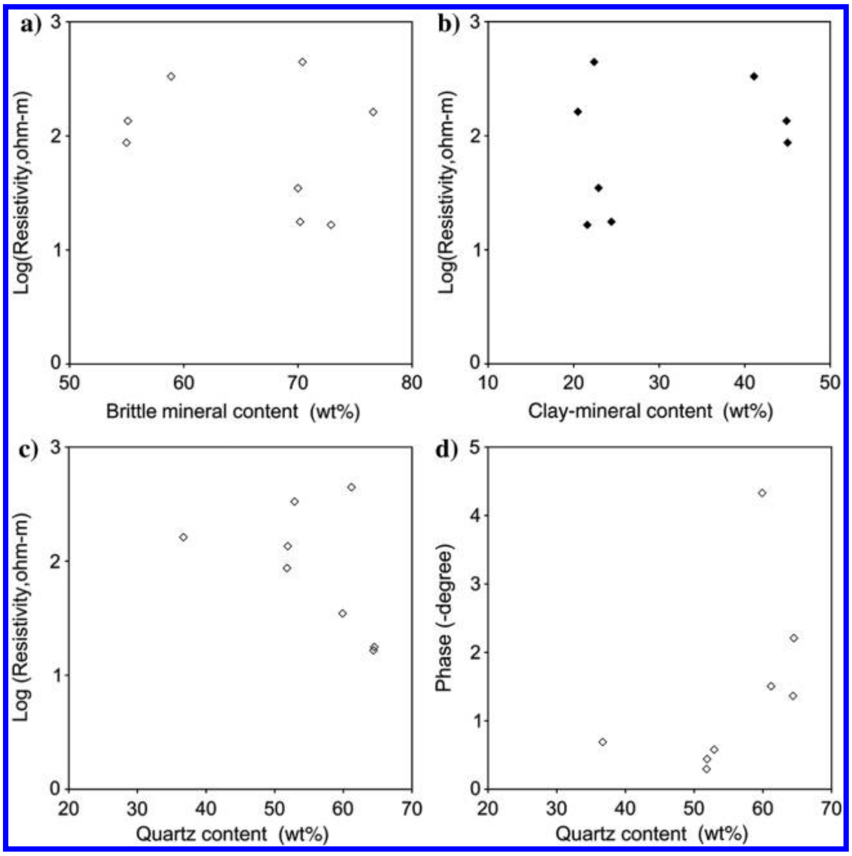

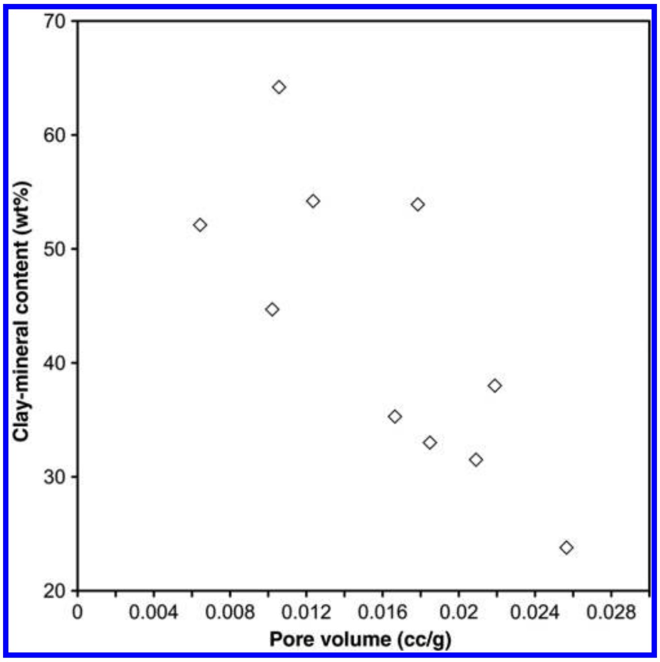

Figure 13. Correlation between the porosity in term of pore volume (cm^3/g) to the clay content of OSH in the Upper Yangtze shows that the pore volume increases with the decreasing clay content. The pore volume is measured by the nitrogen-adsorption method. The result is of different samples from the Chengdu University of Technology.

evidence that the magnitude of interfacial polarization is determined primarily by surface area per unit pore volume (Weller et al., 2015).

Potential applications

A vital issue of using the EM method in shale-gas exploration and developing is understanding the EM property of the sweet spot of a shale-gas play (Wang et al., 2016c). Correlations among the clay mineral, brittle mineral, TOC content, pyrite content, and the complex conductivity of gas shale provide us a new way to evaluate the organic shale. On the one hand, we can improve the logging method to be more useful in estimating the TOC content by measuring the complex conductivity. Our study on electrical properties and its correlation to the petrology of the Upper Yangtze organic shale shows that the TOC varies with the phase of the complex resistivity at lower frequency range. So, complex logging should work well at this frequency range. On the other hand, the clay mineral, brittle mineral, TOC content, pyrite content bear correlation to the reservoir evaluation (sweet-spot delineation) of shale gas. Based on this, we can improve EM methods and refine our understanding of EM data in shale-gas exploration.

CONCLUSION

We conducted a study on the electrical properties and their correlation to the petrology, especially the components of the organic shales, from the Silurian Longmaxi and Cambrian Niutitang Formations in the Upper Yangtze region. Electrical properties connect the EM observation to the geologic interpretation of organic shale. Our study refined our understanding of the electrical properties correlated to the petrology of the organic shales, although there is still much work to do. The organic shales from the research area are characterized by low resistivity and high polarizability in terms of the high negative phase of the complex resistivity, but there is no obvious resistivity low among shaly sandstone, shales with lower and higher TOC. Our study indicates that the pyrite and quartz contents in the shale samples contribute to its low resistivity and high polarizability; the pyrite characterizes itself by conductivity and high polarizability, the quartz content takes effect by improving the porosity of the organic shale in the Upper Yangtze. Our study shows that the petrology parameters of the organic shale, such as TOC, pyrite, and brittle mineral contents bear relations to their electrical properties in terms of the resistivity (conductivity) and phase. It potentially provide a new way to evaluate the parameters of shale gas using the ground-based EM method and helps to delimit the more productive reservoirs (sweet spots), and then to challenge the complex geology, topography, and surface conditions for shale-gas exploration in China, especially in the Upper Yangtze region.

ACKNOWLEDGMENTS

Great thanks go to the associate editor E. Saenger, the assistant editor V. Socco, reviewers Y. G. Li, and two anonymous reviewer for their insightful comments, which have greatly improved the manuscript. Many thanks are due to X. M. Hu (Nanjing University), C. H. Zhang (Oil and Gas Survey of the CGS), Z. X. He, X. J. Liu, G. Yu, and Y. M. Zhou (BGP) for their hard work and help with this project. This research was supported by the National Natural Science Foundation of China (U1262206 and 41502111), the China Geological Survey (DD20160193), and the National Science and Technology Program (2011ZX05019-007).

REFERENCES

Adao, F., O. Ritter, and E. Spangenberg, 2015, The electrical conductivity of Posidonia black shales: From magnetotelluric exploration to rock samples: Geophysical Prospecting, **63**, 1, doi: 10.1111/gpr.2015.63.issue-1.

Alexander, T., J. Baihly, C. Boyer, B. Clark, V. Jochen, J. L. Calvez, R. Lewis, J. Thaeler, and B. E. Toelle, 2011, Shale gas revolution: Oilfield Reviews, **23**, 40–55.

AMETEK.Inc, 2015, 1260A Impedance Analyzer: http://www.ameteksi.com/products/frequency-response-analyzers/1260a-impedance-analyzer, accessed 23 April 2017.

Bowker, K. A., 2007, Barnett Shale gas production, Fort Worth Basin: Issues and discussion: AAPG Bulletin, **91**, 523–533, doi: 10.1306/06190606018.

Fox, R.W., 1830, On the electro-magnetic properties of metalliferous veins in the mines of Cornwall: Philosophical Transactions of the Royal Society, **120**, 399–414, doi: 10.1098/rstl.1830.0027.

Gai, S. H., H. Q. Liu, S. L. He, S. Y. Mo, and J. R. Gu, 2016, Shale reservoir characteristics and exploration potential in the target: A case study in the Longmaxi Formation from the southern Sichuan Basin of China: Journal of Natural Gas Science and Engineering, **31**, 86–97.

Hart, B., C. M. Sayers, and A. Jackson, 2011, An introduction to this special section: Shales: The Leading Edge, **30**, no. 3, 272–273.

He, Z. X., W. B. Hu, and W. B. Dong, 2010, Petroleum electromagnetic prospecting advances and case studies in China: Surveys in Geophysics, **31**, 207–224.

He, Z. X., W. B. Hu, L. G. Xu, and W. L. Li, 2012, Feasibility of monitoring hydraulic fracturing using time-lapse audio-magnetotellurics: Geophysics, **77**, no. 4, WB119–WB126, doi: 10.1190/geo2011-0378.1.

Hill, R. J., E. Zhang, B. J. Katz, and Y. Tang, 2007, Modeling of gas generation from the Barnett Shale, Fort Worth Basin, Texas: AAPG Bulletin, **91**, 501–521, doi: 10.1306/12060606063.

Jackson, L. L., F. W. Brown, and S. T. Neil, 1987, Major and minor elements requiring individual determination, classical whole rock analysis, and rapid rock analysis: Methods for geochemical analysis: U.S. Geological Survey 1770, G1–G23.

Ji, W. M., Y. Song, Z. X. Jiang, L. Chen, Z. Li, X. Yang, and M. M. Meng, 2015, Estimation of marine shale methane adsorption capacity based on experimental investigations of Lower Silurian Longmaxi formation in the Upper Yangtze Platform, south China: Marine and Petroleum Geology, **68**, 94–106, doi: 10.1016/j.marpetgeo.2015.08.012.

Jin, Z. J., Z. Q. Hu, B. Gao, and J. H. Zhao, 2016, Controlling factors on the enrichment and high productivity of shale gas in the Wufeng-Longmaxia Formations, southeastern Sichuan Basin: Earth Science Frontiers, **23**, 1–10.
Karato, S. I., and D. J. Wang, 2013, Electrical conductivity of minerals and rocks, *in* S. I Karato, ed., Physics and chemistry of the deep earth: Wiley-Blackwell, 145–182.
Kuila, U., D. K. McCarty, A. Derkowski, T. B. Fischer, and M. Prasad, 2014, Total porosity measurement in gas shales by the water immersion porosimetry (WIP) method: Fuel, **117**, 1115–1129, doi: 10.1016/j.fuel.2013.09.073.
Kumar, D., and G. M. Hoversten, 2012, Geophysical model response in a shale gas: Geohorizons, **17**, 31–37.
Latovikova, M., 1983, Laboratory measurements of electrical properties of rocks and minerals: Geophysical Surveys, **6**, 201–213, doi: 10.1007/BF01454001.
LECO Corporation, 2008, CS230 Carbon/Sulfur Determinator Specification Sheet: http://www.usbioecuador.com/descargas/leco-inorganica/CS230-ht.pdf, accessed 20 April 2017.
Li, P. F., L. J. Yan, G. Yu, X. J. Liu, and Z. G. Wang, 2015, Induced polarization study based on marine rich organic shale in Southern China: International Workshop and Gravity, Electrical & Magnetic Methods and their Applications, Society of Exploration Geophysicists and Chinese Geophysical Society, 281–284, doi: 10.1190/GEM2015-073.
Li, P. F., L. J. Yan, G. Yu, and Z. G. Wang, 2014, The complex resistivity based on high TOC marine shale formation (in Chinese with English abstract): Journal of Oil and Gas Technology, **36**, 115–119.
Li, Y. B., Y. Li, B. Q. Wang, Z. E. Chen, and D. Nie, 2016, The status quo review and suggested policies for shale gas development in China: Renewable and Sustainable Energy Reviews, **59**, 420–428, doi: 10.1016/j.rser.2015.12.351.
Liu, X. J., Y. M. Zhou, Y. S. Zhu, F. Liu, and C. H. Zhang, 2015, Exploration of organic rich shales using a time-frequency electromagnetic method: International Workshop and Gravity, Electrical & Magnetic Methods and Their Applications, 45–48.
Loucks, R. G., and S. C. Ruppel, 2007, Mississippian Barnett Shale: Lithofacies and depositional setting of a deep-water shale-gas succession in the Fort Worth Basin, Texas: AAPG Bulletin, **91**, 579–601, doi: 10.1306/11020606059.
Luo, Y. Z., and G. Q. Zhang, 1987, Theory and application of spectral induced polarization: SEG.
McCarthy, K., K. Rojas, M. Niemann, D. Palrnowski, and K. Peters, 2011, Basic petroleum geochemistry for source rock evaluation: Oilfield Review, **23**, 32–43.
Meju, M. A., 2002, Geo-electromagnetic exploration for natural resources: Models, case studies and challenges: Surveys in Geophysics, **23**, 133–206, doi: 10.1023/A:1015052419222.
Miller, M., and K. Shanley, 2010, Petrophysics in tight gas reservoirs-key challenges still remain: The Leading Edge, **29**, 1464–1469, doi: 10.1190/1.3525361.
Min, G., X. B. Wang, B. Zhang, Q. Yu, and W. Wei, 2014, A shale gas exploration test with AMT method in Cengong area, northeast Guizhou (in Chinese with English abstract): Oil Geophysical Prospecting, **49**, 815–824.
Nekut, A. G., and B. R. Spies, 1989, Petroleum exploration using controlled-source electromagnetic methods: Proceedings of the IEEE, **77**, 338–362, doi: 10.1109/5.18630.
Nie, H. K., X. Tang, and R. K. Bian, 2009, Controlling factors for shale gas accumulation and prediction of potential development area in shale gas reservoir of South China (in Chinese with English abstract): Acta Petroei Sinica, **30**, 484–491.
Okay, G., P. Leroy, A. Ghorbani, and A. Revil, 2014, Spectral induced polarization of clay-sand mixtures: Experiments and modeling: Geophysics, **79**, no. 6, E353–E375, doi: 10.1190/geo2013-0347.1.
Pan, L., X. Xiao, H. Tian, Q. Zhou, and P. Cheng, 2016, Geological models of gas in place of the Longmaxi shale in Southeast Chongqing, South China: Marine and Petroleum Geology, **73**, 433–444, doi: 10.1016/j.marpetgeo.2016.03.018.
Pan, S. Q., C. N. Zou, Z. Yang, D. Z. Dong, Y. M. Wang, and Z. Y. Wang, 2015, Methods for shale gas play assessment: A comparison between Silurian Longmaxi Shale and Mississippian Barnett Shale: Journal of Earth Science, **26**, 285–294, doi: 10.1007/s12583-015-0524-0.
Parkhomenko, E. I., 1967, Electrical properties of rocks: Plenum Press, 314.
Passey, Q. R., K. M. Bohacs, W. L. Esch, R. Klimentidis, and S. Sinha, 2010, From oil-prone source rock to gas-producing shale reservoir-geologic and petrophysical characterization of unconventional shale-gas reservoirs: International Oil and Gas Conference and Exhibition in China Society of Petroleum Engineers, SPE 131350, 1–29.
Passey, Q. R., S. Creaney, J. B. Kulla, F. J. Moretti, and J. D. Stroud, 1990, A practical model for organic richness from porosity and resistivity logs: AAPG Bulletin, **74**, 1777–1794.
Phillips, C. R., 2010, Experimental study of the induced polarization effect using Cole-Cole and GEMTIP models: M.S. thesis, University of Utah.
Pirson, S. J., 1971, New electric technique can locate gas and oil: World Oil, **172**, 69.
Polish Geological Institute, 2012, Assessment of the shale gas and shale oil resources of the lower Paleozoic Baltic-Podlasie-Lublin basin in Poland, http://www.pgi.gov.pl/pl/dokumenty-in/doc_view/769-raport-en.html, accessed 19 February 2014.
Ran, W., 2015, Study on the petrology response of the shale-gas reservoir: Master thesis, Southwest Petroleum University.
Rust, W. M., 1940, Typical electrical prospecting methods: Geophysics, **5**, 243–249, doi: 10.1190/1.1441807.
Seaton, N. A., and J. P. R. B. Walton, 1989, A new analysis method for the determination of the pore size distribution of porous carbons from nitrogen adsorption measurements: Carbon, **27**, 853–861, doi: 10.1016/0008-6223(89)90035-3.
Slater, L. D., J. Y. Choi, and Y. X. Wu, 2005, Electrical properties of iron-sand columns: Implications for induced polarization investigation and performance monitoring of iron-wall barriers: Geophysics, **70**, no. 4, G87–G94, doi: 10.1190/1.1990218.
Tang, X. L., Z. X. Jiang, H. X. Huang, S. Jiang, L. Yang, F. Y. Xiong, L. Chen, and J. Feng, 2016, Lithofacies characteristics and its effect on gas storage of the Silurian Longmaxi marine shale in the southeast Sichuan Basin, China: Journal of Natural Gas Science and Engineering, **28**, 338–346, doi: 10.1016/j.jngse.2015.12.026.
Ulrich, C., and L. D. Slater, 2004, Induced polarization measurements on unsaturated, unconsolidated sands: Geophysics, **69**, 762–771, doi: 10.1190/1.1759462.
U.S. Energy Information Administration, 2013, Technically recoverable shale oil and shale gas resources: An assessment of 137 shale formations in 41 countries outside the United States.
Wang, R. Y., W. L. Ding, Y. Q. Zhang, Z. Wang, X. H. Wang, J. H. He, W. T. Zeng, and P. Dai, 2016a, Analysis of developmental characteristics and dominant factors of fractures in Lower Cambrian marine shale reservoirs: A case study of Niutitang formation in Cen'gong block, southern China: Journal of Petroleum Science and Engineering, **138**, 31–49, doi: 10.1016/j.petrol.2015.12.004.
Wang, X. B., B. Zhang, Z. X. He, L. F. He, K. Yang, T. Huang, F. B. Luo, J. L. Tang, and L. Gan, 2016c, Electrical properties of Longmaxi organic-rich shale and its potential applications to shale gas exploration and exploitation: Journal of Natural Gas Science and Engineering, **36**, 573–585, doi: 10.1016/j.jngse.2016.10.027.
Wang, Y., X. Li, Z. H. Zhao, R. Q. Zhou, B. Zhou, and G. F. Li, 2016b, Contributions of non-tectonic micro-fractures to hydraulic fracturing: A numerical investigation based on FSD model: Science China Earth Sciences, **59**, 851–865, doi: 10.1007/s11430-015-5232-1.
Wang, Y. M., D. Z. Dong, J. Z. Li, S. J. Wang, X. J. Li, L. Wang, K. M. Cheng, and J. L. Huang, 2012, Reservoir characteristics of the shale gas in Longmaxi Formation of the lower Silurian, southern Sichuan (in Chinese with English abstract): Acta Petroei Sinica, **33**, 551–561.
Weller, A., L. Slater, J. A. Huisman, O. Esser, and F. H. Haegel, 2015, On the specific polarizability of sands and sand-clay mixtures: Geophysics, **80**, no. 3, A57–A61, doi: 10.1190/geo2014-0509.1.
Wu, Q. H., X. B. Li, H. L. Liu, and X. Chen, 2011, Log interpretations and the application of core testing technology in the shale gas: Taking the exploration and development of the Sichuan Basin as an example: Acta Petrolei Sinica, **32**, 484–488.
Yan, J. F., Y. P. Men, Y. Y. Sun, Q. Yu, W. Liu, H. Q. Zhang, J. Liu, J. W. Kang, S. N. Zhang, H. H. Bai, and X. Zheng, 2016, Geochemical and geological characteristics of the Lower Cambrian shales in the middle upper Yangtze area of South China and their implication for the shale gas exploration: Marine and Petroleum Geology, **70**, 1–13, doi: 10.1016/j.marpetgeo.2015.11.010.
Xiang, K., W. B. Hu, L. J. Yan, C. H. Zhang, W. H. He, X. G. Tang, and L. X. J. Liu, 2014, Complex resistivity dispersion characteristics of shale samples in Sichuan and Guizhou area (in Chinese with English abstract): Oil Geophysical Prospecting, **49**, 1013–1019.
Xiang, K., W. B. Hu, G. Yu, L. J. Yan, X. G. Tang, and H. Hu, 2016, Prediction of TOC in shale gas reservoir by using complex resistivity method: Workshop: Rock Physics and Borehole Geophysics, 17–20, doi: 10.1190/RP2016-005.
Yan, L. J., K. Xiang, P. F. Li, and Z. G. Wang, 2014, Study on the induced polarization model in the exploration for shale gas in southern China: 84th Annual International Meeting, SEG, Expanded Abstracts, 912–916.
Yang, F., Z. F. Ning, Q. Wang, and H. Q. Liu, 2016, Pore structure of Cambrian shales from the Sichuan Basin in China and implications to gas storage: Marine and Petroleum Geology, **70**, 14–26, doi: 10.1016/j.marpetgeo.2015.11.001.
Yang, R. D., S. J. Wang, L. M. Dong, L. J. Jiang, W. H. Zhang, and H. Gao, 2003, Sedimentary and geochemical characteristics of Sinian cap carbonates in the Upper Yangtze region: Chinese Journal of Geochemistry, **22**, 320–341, doi: 10.1016/j.apgeochem.2006.11.005.
Yu, G., Z. X. He, L. F. He, T. P. Wang, W. B. Hu, K. Xiang, H. Hu, and P. F. Li, 2014, Complex resistivity characteristics of high TOC marine shale

core samples and its applications: 84th Annual International Meeting, SEG, Expanded Abstracts, 2964–2968.

Yu, G., Z. X. He, L. F. He, T. P. Wang, W. B. Hu, K. Xiang, H. Hu, and P. F. Li, 2015, Complex resistivity characteristics of high TOC marine shale core samples and its applications: GEM Chengdu 2015 : International Workshop on Gravity, Electrical & Magnetic Methods and Their Applications , 41–44.

Yu, G., W. B. Hu, Z. X. He, K. Xiang, H. Hu, and P. F. Li, 2016, High TOC shale core samples complex resistivity measurement and its applications: International Conference and Exhibition, Barcelona, 333.

Zhang, B. M., S. C. Zhang, L. Z. Bian, Z. J. Jin, and D. R. Wang, 2007, Developmental modes of the Neoproterozoic-Lower Paleozoic marine hydrocarbon source rocks in China: Chinese Science Bulletin, **52**, 77–91, doi: 10.1007/s11434-007-6018-4.

Zhang, C. H., X. J. Liu, L. F. He, and W. H. He, 2013, A study of exploration organic rich shales using time-frequency electromagnetic method (TFEM): Chinese Journal of Geophysics-Chinese Edition, **56**, 3173–3183.

Zhdanov, M. S., 2010, Electromagnetic geophysics: Notes from the past and the road ahead: Geophysics, **75**, no. 5, 75A49–75A66, doi: 10.1190/1.3483901.

Zhou, Y. M., X. J. Liu, C. H. Zhang, and Y. S. Zhu, 2015, The TEEM technology for quick identification of "sweet spot" of shale gas and its applications: Geophysical and Geochemical Exploration, **39**, 60–63.

Zhu, Y. P., E. R. Liu, A. Martinez, M. A. Payne, and C. E. Harris, 2011, Understanding geophysical responses of shale-gas plays: The Leading Edge, **30**, no. 3, 332–338.

Zonge, K. L., 1972, Electrical properties of rocks as applied to geophysical prospecting: Ph.D. thesis, The University of Arizona.

Zou, C. N., D. Z. Dong, and Y. M. Wang, 2015, Shale gas in China: Characteristics, challenges and prospects (I): Petroleum Exploration Development, **42**, 753–767, doi: 10.1016/S1876-3804(15)30072-0.